Importance of non-stationary analysis for assessing extreme sea levels under sea level rise

Damiano Baldan[1], Elisa Coraci[1], Franco Crosato[1], Maurizio Ferla[1], Andrea Bonometto[1], Sara Morucci[1]

[1]Italian Institute for Environmental Protection and Research, ISPRA, Venice, Italy

Correspondence to: Sara Morucci (sara.morucci@isprambiente.it)

Abstract. Coastal flooding caused by extreme sea levels (ESLs) is one of the major impacts related to the climate change. It is expected to increase in the future due to sea level rise and storm surge intensification. Estimates of return levels obtained under the framework provided by extreme events theory might be biased under climatic non-stationarity. Additional uncertainty is related to the choice of the model. In this work, we fit several extreme values models to a long-term (96 years) sea level record from the city of Venice (NW Adriatic Sea, Italy): a Generalized Extreme Value distribution (GEV), a Generalized Pareto Distribution (GPD), a Point Process (PP), the Joint Probability Method (JPM), and the Revised Joint Probability Method (RJPM) under different detrending strategies. We model non-stationarity with a linear dependence of the model's parameters from the mean sea level. Our results show that non-stationary GEV and PP models fit the data better than stationary models even with detrended data. The non-stationary PP model is able to reproduce the rate of extremes occurrence fairly well. Actualized estimates of the return levels for non-stationary and detrended models are generally higher than estimates from stationary, non-detrended models. Thus, projections of return levels in the future might be significantly different from those calculated using stationary models. Overall, we show that non-stationary extremes analyses can provide more robust estimates of return levels to be used in coastal protection planning.

Eliminato: and

Eliminato: models

1. Introduction

Coastal zones are extremely vulnerable to extreme sea levels (ESLs; Kron, 2013). Exposure to coastal flooding damage is projected to increase in the future (Jongman et al., 2012) due to higher frequency, magnitude, and duration of extreme sea levels (Tebaldi et al., 2021; Devlin et al., 2021). Relevant causes are the mean sea level rise (Menéndez and Woodworth, 2010; Marcos et al., 2009), and increases in storm surges intensity (Cid et al., 2016; Vousdoukas et al., 2016). The design of structures to protect coasts from flooding (minimizing e.g. damages to infrastructures and coastal erosion) relies on the knowledge of ESLs that are likely to occur with a given probability (Boettle et al., 2016). Extreme events theory provides a theoretical background to fit historical extremes with specific probability distribution functions (Coles et al., 2001), and is widely used for estimating the probability of occurrence of ESLs. However, two challenges complicate the development of solid estimates of such return levels.

The first challenge is linked to the potential non-stationary behavior of the extremes. The results of extreme value theory are valid under the assumptions of independence and stationarity of extremes (Khaliq et al., 2006). Here, stationarity means that all the realizations of the extremes in the data record are generated from the same distribution (Coles et al., 2001). While independence is satisfied with a proper selection of extremes from the dataset, stationarity is often assumed but not verified (Khaliq et al., 2006). When dealing with sea level data, several sources of non-stationarity exist, e.g.: changes in coastal morphology, low frequency climatic variability, and climate change (Salas and Obeysekera, 2014). Assuming stationarity when data are non-stationary has several practical implications. First, this choice can greatly affect the return levels estimated for the present day (Razmi et al., 2017; Dixon and Tawn, 1999; Salas and Obeysekera, 2014; Haigh et al., 2010; Ragno et al., 2019). Non-stationary analyses can lead to very different estimates of the return levels used for designing structures. For instance, when a 100-years return level is used for the design, it has to be ensured that the value remains valid until the end of the structure's lifetime (Mudersbach and Jensen, 2010). The estimation of return levels from stationary models might not be appropriate because of the implicit assumptions that the characteristics of the extremes remains the same in the future (Caruso and Marani, 2022).

Several methods were proposed to cope with non-stationary conditions. Records whose length is limited to some decades could be too short to show non-stationary patterns (Marcos et al., 2009). When the main source of non-stationarity is the mean sea level change, detrending with annual or long term means is an option (Bernier et al., 2007; Tebaldi et al., 2012; Mentaschi et al., 2016). However, detrending implicitly attributes the causes of non-stationariety to a single factor (i.e. the mean sea level), while other causes might be overlooked (Arns et al., 2017). When sufficient amount of data is available, the extreme value distribution that generates the extremes can be explicitly modeled as dependent from non-stationary factors such as seasonality (Méndez et al., 2007), meteorology (Grinsted et al., 2013), climate (Cid et al., 2016), sea level rise (Sweet and Park, 2014), and time (Razmi et al., 2017). However, clear indications on which approach suits better non-stationary conditions are still missing.

The second challenge is related to the choice of the proper method to conduct the extreme sea level analysis. Several methods exist, direct (i.e. parametric, based on fitting theoretical Probability Distribution Functions, PDFs, to the data), and non-direct (using mixtures of empirical and parametric PDFs). Several theoretical PDFs were derived based on different methods to identify the extreme values in the data (e.g. maxima over blocks of data, or values that exceed a threshold, Coles et al. 2001): Generalized Extreme Value distributions (Mudersbach and Jensen, 2010), Generalized Pareto distributions (Wahl et al., 2017), and Point Process (Boettle et al., 2016). Indirect methods such as the Joint Probability Method, or the Revised Joint Probability Method (Pugh and Vassie, 1978) also exist. It is expected that different methods might be more or less suited (in terms of explained variance, see section 2.3.6) to accommodate non stationary data, and might lead to different estimates of extreme sea level probabilities (Wahl et al., 2017; Razmi et al., 2017). However, a comparison of the suitability of different methods for modelling non-stationarity is currently missing.

Given the above knowledge gaps, this paper aims at: (i) assessing which parametric method best accommodates non-stationary conditions; and (ii) comparing return level and return period estimates from different parametric and non-

Eliminato: (
Eliminato:)
Codice campo modificato
Codice campo modificato
Eliminato: (
Eliminato:)
Eliminato: parametric
Eliminato: non parametric
Eliminato: Non-parametric
Eliminato: modeling

parametric methods. We perform all the analyses using three different detrending strategies. We use a long-term sea level time series (96 years) recorded at Venice, Punta della Salute station (NE Italy). We compare the implemented methods also for sea level data from the tide gauge in Marseille (Southern France).

2. Methods

2.1 The Venice Lagoon

The Venice lagoon is the largest Mediterranean lagoon, covering a length of 50 km along the coast, with an area of 500 km^2. The lagoon is connected to the sea by three inlets (Lido, Malamocco and Chioggia). The tide regime is semi-diurnal, with mean tidal range from 50 cm during neap tide to 100 cm during spring tide (Umgiesser et al., 2021). Around 415 km^2 are subject to tide excursion, and a large area (~2400 km^2) in the surrounding coastline lies below the mean sea level. Sea level in the Venice lagoon is determined by the tide and the meteorological surge, driven by atmospheric phenomena at different spatial scales (Lionello et al., 2021). Among the atmospheric contributions, storm surge is the dominant driver of extreme sea levels (Ferrarin et al., 2022), and is controlled predominantly by the local atmospheric pressure and the wind (Bora from north-east and Sirocco from south-east are predominant).

Due to the semi-closed shape of the Adriatic Sea, the Venice Lagoon is exposed to the risk of flooding due to extreme sea levels (ESLs, Ferrarin et al., 2022). Compared to other sites in the northern Adriatic sea, the Venice Lagoon experienced higher sea level rise due to the combined effects of subsidence and eustatism (+ 2.5 mm $year^{-1}$ in the last 150 years, Biasio et al., 2020; Zanchettin et al., 2021). The current long-term mean sea level is about 30 cm above the local 1897 reference (named Zero Mareografico di Punta della Salute, ZMPS: average sea level for the period 1885-1909 measured at the Punta della Salute gauging station). As a result, an increase in the frequency and magnitude of ESLs causing flooding of the city of Venice was recorded (Umgiesser et al., 2021). Additionally, morphological changes (Carniello et al., 2009) affected the propagation of tide waves in the lagoon (Lionello et al., 2021). The events with the highest recorded sea levels occurred on November 4th, 1966 (+ 194 cm), and November 12th, 2019 (+ 189 cm, Lionello et al., 2021).

On the contrary, area where the Marseille tide gauge is located has a lower tidal range (around 10 cm, Fig S1), and is located on a stable background, with a relative sea level rise of + 1.1 mm y^{-1} in the last 150 years (Letetrel et al., 2010; Wöppelmann et al., 2014).

2.2 Tide gauge data

We used sea level data recorded by the tide gauge station located in Venice (gauge name: *Punta della Salute*) covering the period 1924 – 2019. Data from 2020 onwards are affected by the activation of a storm surge barrier system that prevents ESLs to propagate inside the Venice lagoon (MOSE) and therefore were not included in the analysis. This is one of the three longest sea level time series in the Mediterranean Sea (Venezia, Genova, Marseille). The float-operated tide gauge is located inside a still well; measurements were recorded mechanically until 1988 and electronically from 1989 onwards. Until 1989,

Formattato: Apice
Formattato: Apice
Formattato: Apice
Formattato: Apice
Formattato: Apice
Eliminato: ¶
Formattato: Tipo di carattere: Corsivo
Eliminato: T
Eliminato: Marsiglia
Eliminato:

semidiurnal maxima and minima are available (4 measurements per day); then data were recorded hourly in the period 1989 - 1994, every half hour in 1995 - 2006, every ten minutes in 2007 - 2019. The data have no gaps; a total record length of 96 years was used to fit the models. To calculate long-term mean sea level before 1924, we used yearly mean sea level data from other tide gauge stations active in the city of Venice (and thus affected by the same subsidence rate as *Punta della Salute*) whose records cover the period 1885 – 1922 (namely: *Campo Santo Stefano*, *Arsenale*, and *Punta della Salute – Canal Grande*; for details see Zanchettin et al., 2021).

Hourly sea level data recorded at Marseille are available for the time period 1849 – 2017. Measurements were performed with a float-operated tide gauge until 1988, with an acoustic sensor for 1989 – 2008, and with a radar sensor from 2009 onwards. measurements were recorded mechanically until 1988 and electronically from 1989 onwards (Wöppelmann et al., 2014). A total record length of 77 years (spanning 1903 - 2017) was used to fit the model, since some years were discarded due to incomplete records.

2.2.1 Data detrending

We used two different strategies for detrending the sea level data before fitting the models: a) we removed from each sea level observation the yearly average mean sea level (hence after: MSL detrending); b) we removed from each sea level observation the sea level average calculated over the previous 19 years (hence after: MSL_L detrending), to remove long term fluctuations due to interferences between lunar precession and solar activity (Valle-Levinson et al., 2021); c) we used non detrended data to fit the models (hence after: NDT).

2.3 Extreme Values distributions

Extreme events are defined as events with a low probability of occurrence (Coles et al., 2001). Given a set of independent and identically distributed random variables $X_1, \dots, X_n$, with parent distribution F, a probability distribution function describing the occurrence probability of extreme values can be derived with two approaches. The Block Maxima (BM) approach considers the distribution of the maxima of the set $X_1, \dots, X_n$ over blocks of length n: $M_n = max\{X_1, \dots, X_n\}$ and assesses $Pr(M_n < z)$, i.e. the probability that the random variable M_n is greater than z. The use of sufficiently large blocks ensures that the maxima are independent (Méndez et al., 2007). The Peaks Over Threshold (POT) approach assesses $\Pr(X > u + y \mid X > u)$, i.e. the probability that the random variable X exceeds a sufficiently high threshold u by the value y. When fitting POT, an appropriate threshold needs to be selected to properly model excesses as extremes (Zhang et al., 2000). In this work, we used a block length of one year to extract BM to fit the GEV models. We selected the threshold for POT models (GPD and PP) with a two-step approach. First, data above the 99th percentile were selected, and events separated by more than 78 hours were considered independent and retained. This time span corresponds to the average decay time of seiches, the lowest-frequency sub seasonal oscillation in the Northern Adriatic sea (Masina and Ciavola, 2011; Raicich et al., 1999). Second, we fitted multiple POT models based on different thresholds, and we selected the lowest value that ensures the stability of the GPD and PP parameters. This procedure ensures that the threshold excesses can be properly modeled as

Eliminato:
Formattato: Tipo di carattere: Corsivo
Eliminato: -
Formattato ...
Eliminato: (
Formattato ...
Eliminato: X_1,…,X_n
Eliminato: F
Formattato ...
Eliminato: X_1,…,X_n
Formattato: Tipo di carattere: Corsivo
Formattato ...
Eliminato: M_n=max{X_1,…,X_n }
Eliminato: Pr(M_n<z)
Formattato ...
Eliminato: M_n
Formattato: Tipo di carattere: 10 pt
Formattato ...
Formattato: Tipo di carattere: Corsivo
Formattato ...
Eliminato: Pr(X>u+y | X>u)
Formattato ...

extremes, and eq. 2 holds (Coles et al., 2001). Thresholds of 100 and 80 cm are appropriate to select POT for non-detrended and detrended data, respectively, yielding 319 POT for NDT, 284 for MSL, and 359 for MSL_L.

2.3.1 Generalized Extreme Value Distribution

The BM distribution depends on F, the parent distribution of the random variables in each block via: $G(z) = Pr(M_n < z) = F^n(z)$, converging to the generalized extreme values (GEV) distribution when n is large enough (Coles et al., 2001):

$$G(z) = exp\left[-\left\{1 + \xi\left(\frac{z-\mu}{\sigma}\right)\right\}_+^{-1/\xi}\right] \quad (1)$$

where $a_+ = \max(a, 0)$, μ is the location parameter (proportional to the first-order moment of the distribution), σ is the scale parameter (always positive, proportional to the second-order moment of the distribution), and ξ is the shape parameter that determines the type of distribution function: the heavy-tailed Frechet (ξ > 0), the upper-bounded Weibull (ξ < 0), and the limit-case Gumbel (ξ → 0).

2.3.2 Generalized Pareto Distribution

The POT distribution depends on F, the parent distribution of the random variables via: $H(y) = \Pr(X > u + y \mid X > u) = (1 - F(u + y)/(1 - F(u))$, with $y=z-u$, converging to the Generalized Pareto Distribution (GPD) when the threshold is large enough (Coles et al., 2001):

$$H(z) = 1 - \left[1 + \xi\left(\frac{z-u}{\sigma_u}\right)\right]_+^{-1/\xi} \quad (2)$$

where u is the threshold, σ_u is the GPD scale parameter dependent on the threshold, and ξ the shape parameter that determines the type of the distribution function: heavy-tailed Pareto (ξ > 0), upper bounded Beta (ξ < 0), with the Exponential as limit-case (ξ → 0). When BM are GEV-distributed, POT is theoretically expected to follow a GPD with the same shape parameter and scale depending on the GEV parameters $\sigma_u = \sigma + \xi(u - \mu)$ (Gilleland and Katz, 2016). This property can drive the selection of an appropriate threshold u.

2.3.3 Point process approach

The occurrence of POT can be modeled also as a point process. Under stationary conditions, the process follows a Poisson distribution (Coles et al., 2001; Menéndez and Woodworth, 2010):

$$O(k) = \Pr(X = k) = \frac{\lambda^k e^{-k}}{k!} \quad (3)$$

where λ is the rate of the process (number of events over a reference time period). The process rate depends on the GEV parameters (Gilleland and Katz, 2016; Boettle et al., 2016; Cid et al., 2016):

$$\lambda = \left[1 + \xi\left(\frac{z-\mu}{\sigma}\right)\right]_+^{-1/\xi} \quad (4)$$

Formattato: Tipo di carattere: Corsivo

Formattato: Tipo di carattere: 10 pt

Eliminato: u

Formattato: Tipo di carattere: 10 pt

Formattato: Tipo di carattere: 10 pt

Eliminato: σ_u

When location and scale are not constant (e.g. a dependence from a covariate is introduced), the point process is non homogeneous (Cebrián et al., 2015).

2.3.4 Joint Probability and Revised Joint Probability methods

Unlike the methods mentioned above, the joint probability method (JPM) is non-parametric. The JPM is based on the decomposition of the sea level z in the tide (x) and surge (y) components (Pugh and Vassie, 1978). The probability distribution of the sea level P(z) results from the convolution of the distributions of the tide and the surge:

$$P(z) = \int_{-\infty}^{+\infty} P_T(z-y)\, P_S(y)\, dy \quad (5)$$

where $z = x + y$, $P_T(x)$ is the distribution of the tide, and $P_S(y)$ is the distribution of the surge (both obtained from hourly records), assumed to be independent (Marcos et al., 2009).

The revised Joint Probability Method (RJPM) improves the JPM by fitting the surge distribution with a probability distribution function, to allow for the smoothing of the empirical distributions, and for projections beyond the highest measured surge (Tawn et al., 1989).

For both JPM and RJPM, an extremal index can be calculated to account for dependencies in the hourly data. The extremal index is used as a correction factor in the return period calculation based on $P(z)$ (see section 2.3.7), and is defined as the average number of measurements an extreme sea level cluster is usually composed of (Tawn et al., 1989).

The tidal component of the mean sea level used in the JPM was calculated with the 'oce' package (Kelley, 2018) in the R computing environment v4.1.2 (R Core Team, 2021), using the yearly detrended sea level data (MSL), 7 harmonic constants (M2, S2, N2, K2, K1, O1, P1) for Venice, and 21 harmonic constants for Marseille (Wöppelmann et al., 2014). The surge was calculated as the difference between the sea level observation and the corresponding tide. We used 1990-2019 hourly data from for Venice and 1968-2016 for Marseille (record length of 30 years for both stations).

For the JPM, we used all the tide and surge data from the sea level decomposition to generate the empirical frequency distribution over classes of width 10 cm. The maximum theoretical sea level (sum of maximum tide and maximum surge) falls within the highest class. Then, we calculated the discrete convolution between the two histograms. For the RJPM, and fitted a Gumbel distribution function to the annual maxima of the surge (following Tawn et al., 1989). Then we calculated the probability for each histogram class as the integral of the distribution. The quantiles of the obtained histogram representing the empirical sea level distribution were calculated based on the frequency of each class, and used for the estimation of return levels (Pugh and Vassie, 1978; Marcos et al., 2009). We found extremal indices of 5.5 and 13 to be appropriate for Venice and Marseille, respectively.

2.3.5 Models fitting

We used the package 'ExtRemes' (Gilleland and Katz, 2016) to fit the parametric models (GEV, GPD, PP) based on the Maximum Likelihood criterion (Castillo et al., 2005; Coles et al., 2001).

Eliminato: p
Eliminato: method
Eliminato: methods
Eliminato:
Eliminato: P_T (x)
Formattato: Tipo di carattere: 10 pt
Eliminato: z=x+y
Eliminato: P_S (y)
Formattato: Tipo di carattere: 10 pt
Formattato: Tipo di carattere: 10 pt
Formattato: Tipo di carattere: 10 pt
Formattato: Tipo di carattere: 10 pt
Formattato: Tipo di carattere: 10 pt
Formattato: Tipo di carattere: 10 pt
Eliminato: and
Eliminato: for the fit
Eliminato: We used our own script to generate the empirical sea level distribution function according to the JPM. We first generated the empirical distribution histograms for the tide and the surge using a bin width of 10 cm for the classification, and then we calculated the convolution between the two histograms.
Eliminato: empirical

2.3.5 Stationarity and parameters dependence

Both BM and POT approaches require the modeled random variables to follow the same parent distribution F. Non stationary conditions can be modeled by including covariates in the GEV, GPD, and PP parameters (Méndez et al., 2007). For instance, a linear dependence of location (μ) and scale (σ) parameters can be assumed from the covariate c and can be expressed as (Coles et al., 2001):

$$\mu(c) = \mu_0 + \mu_1 c \quad (6)$$

$$log(\sigma(c)) = \sigma_0 + \sigma_1 c \quad (7)$$

where the logarithm on the scale parameter in eqn. 7 is used to constrain the scale parameter to positive values.

2.3.6 Comparing different models configurations

The likelihood ratio test is employed to assess whether the inclusion of a covariate in the model formulation improved significantly the fit. Two nested competing models $M_0 \subset M_1$ can be compared using the deviance statistic (Coles et al., 2001). For example, M_1 can be a model that whose parameters depend on covariates, while M_0 a model whose parameters do not depend from covariates. The deviance is expressed as:

$$D = 2\{l_1(M_1) - l_0(M_0)\} \quad (8)$$

where $l_1(M_1)$ and $l_0(M_0)$ are the maximized log-likelihoods of models M_1 and M_0, respectively. The model M_0 has by definition a lower complexity than M_1, which is the case when covariates on the model's parameters are added to M_1. High deviance values support the hypothesis of M_1 explaining a larger variation in the data than M_0 (likelihood ratio test). The hypothesis is rejected when $D > c_\alpha$ where c_α is the $(1-\alpha)$ quantile of a χ^2_k distribution, where k is the difference in dimensionality between M_1 and M_0.

2.3.7 Return levels estimation

The return period is defined as: $Tr(z) = [1 - G(z)]^{-1}$, where G is the Probability Distribution Function for the GEV, GPD, or PP models (Caruso and Marani, 2022). In practice, the extreme levels of the random variable are calculated as a function of the return period via the PDF quantiles (Coles et al., 2001). In a non-stationary analysis, the model's PDF is not constant in time (Fig. 1), and the quantiles are not uniquely determined. To allow for the comparison of estimated return levels from non-stationary models, in this work we first fixed the covariates values, and then calculated the quantiles of the resulting probability distribution function.

Formattato: Tipo di carattere: 10 pt
Formattato: Tipo di carattere: 10 pt
Eliminato: M_0⊂M_1
Formattato: Tipo di carattere: 10 pt
Formattato: Tipo di carattere: 10 pt
Formattato: Tipo di carattere: 10 pt
Eliminato: :
Formattato: Interlinea: 1,5 righe
Eliminato: models
Formattato: Tipo di carattere: 10 pt
Formattato: Tipo di carattere: 10 pt
Eliminato: M_1
Eliminato: M_0
Formattato: Tipo di carattere: 10 pt
Formattato: Tipo di carattere: 10 pt
Eliminato: M_0
Eliminato: M_1
Eliminato: M_1
Eliminato: M_0

2.4 Data analysis

Before fitting the models, we employed a Mann-Kendall test to check if BM and POT resulting from different detrending strategies follow a temporal trend. Additionally, we used linear models and quantile regressions (75th quantile) to relate BM and POT with the mean sea level, and used the significance of the regressions as indication for stationarity.

To check if the inclusion of non-stationary covariates can improve the models (objective i), we fitted different configurations of GEV, GPD, and PP models to the full dataset (96 years). We fitted: a) models without covariates; b) models with the location linearly depending on the yearly mean sea level; and c) models with location and logarithm of the scale linearly depending on the yearly mean sea level. We used the likelihood ratio test (eq. 8) to assess whether the inclusion of mean sea level-dependent parameters improved the fit significantly.

To check visually the dependence of parameters from the mean sea level, we fitted stationary GEV, GPD, and PP models (i.e. without covariates on the scale and location parameters) to BM and POT subsets using a 30-years moving time window. We can assume that data sampled in a 30-years window can be considered stationary. We tested for the presence of a trend in the fitted parameters with a Mann-Kendall test. We plotted the sequence of stationary parameters together with non-stationary ones as a mean to visually check the uncertainty related to parameters estimation (Cheng et al., 2014).

The PP models were further validated by comparing the process rate (eq. 4) and the empirical rate of POT exceedances (number of excesses per year) with a Pearson's correlation test.

After fitting the models, we compared the estimates of the return level for different return periods (objective ii). For the non-stationary models, we first calculated the location and scale parameters with a yearly mean sea level of + 35 cm (equal to the 2000 - 2019 long-term mean sea level). Once the model's parameters were fixed, we calculated the sea levels corresponding to return periods of 2, 20, 100, and 200 years. Estimates of return levels from models fitted to detrended data were added back the long term mean sea level. This additive procedure is simplified and neglects the non-linear interactions between future mean sea level and the occurrence of extremes (Arns et al., 2015, 2017).

Finally, we derived the curves from non detrended, non-stationary models under different covariates values. For Venice, we used + 0 cm; + 25 cm (annual mean sea level in 1966, the year of the largest ESL on record); + 35 cm (annual mean sea level for 2019, the last year used in the analysis); and + 51 cm (expected annual mean sea level in 2050 under IPPC scenario SSP2-4.5, Garner et al., 2021; Masson-Delmotte et al., 2021). For Marseille, we used + 54 cm (annual mean sea level for 2019), and + 71 (expected annual mean sea level in 2050 under IPPC scenario SSP2-4.5).

Eliminato: W

3. Results

Regarding the data used to fit the models, the Mann-Kendall tests detected a significant trend for the non-detrended BM, a marginally significant trend for the detrended BM, and no trend for POT for Venice (Fig. 2). We found evidence for a dependence of the median BM on the mean sea level for both detrended and non-detrended data. The median POT, and the upper POT quantile were significantly dependent from the mean sea level only for the MSL_L detrending method (Table 1).

After fitting the models, the likelihood ratio test for Venice data shows that the inclusion of the covariate (mean sea level) improves the fit significantly for the location (μ) parameter of both GEV and PP for NDT and MSL_L data, and only for GEV for MSL data (Table 2). The addition of a dependence on the scale (σ) parameter was marginally significant for the GPD for NDT and MSL_L data. The inclusion of the dependence from the scale on the PP improved the fit only for MSL_L data (Table 2). In Marseille, the inclusion of the covariate improved the fit for the location for GEV and PP for NDT, and for the location of PP for MSL_L data

Models validation for Venice showed that the location parameter dependent on the covariate well reproduces the temporal trends of the corresponding stationary parameters obtained from the time-window analysis in GEV and PP. The location is included in the scale parameter of the GPD that does not improve the fit (Fig. 3). The scale parameter improves the fit only marginally also for GEV and PP.

Additionally, the PP models estimated the occurrence rate of threshold exceedances in Venice in good agreement with those calculated from the POT data (Table 3).

The return levels estimated by non-stationary models for Venice were in the range 133 – 146 cm for a return period of 2 years, 169 – 184 cm for 20 years, 192 – 203 cm for 100 years, and 198 – 218 cm for 200 years (see Table S1 for Venice, and Table S2 for Marseille). Estimates of 100-years return levels for non detrended models with covariates were in the range 169 – 181 cm, while for detrended models without covariates were higher (186 – 187 cm). Models that include covariates on the location showed an increased extreme estimate for smaller return periods (< 10 y for GEV, and < 3 y for PP, Fig. 4), with higher discrepancies for non detrended data.

Finally, we compared how the return levels for return periods of 2, 20, 100, and 200 years differ among models (Fig. 5, Table S1). Among stationary models, the GPD yields conservative estimates for 2 years and the GEV is more conservative for 20 and 100 years for all detrending configurations. Among models with covariates on the location, GEV yields higher return levels estimates. Among non-stationary models fitted to non-detrended data, GPD models with covariate on the scale yield conservative estimates for all return periods. Estimates from GEV models with covariates on location and scale fitted to detrended data are more conservative for 20, 100, and 200 years. The JPM and RJPM yields projections that are in agreement with parametric models. Return levels from models without covariates fitted to non detrended data were consistently the less conservative for all return periods and both Venice and Marseille. The highest differences between detrended, non detrended and stationary models were higher for short return periods. Among all the analysed methods, in Venice the GEV with covariate on the location, the JPM, and RJPM yield the most conservative estimates of return levels for longer return time (>50 yr), while for return time of 2 and 20 years the RJPM is less conservative than other methods. A similar behaviour is observed in Marsille for RJPM. Differently, in Marsille the JMP provides less conservative return level for all return times. A consistent behaviour was observed when stationary models fitted to data covering 30 years were compared with JPM and RJPM (Figure S2).

Extrapolations of non detrended, non-stationary models for the future showed that estimates of future ESLs are strongly influenced by the future mean sea level (Fig. 6). Events that currently have a return level above 200 y are projected to have

Eliminato:
Eliminato: 9
Eliminato: 159
Eliminato: 171
Eliminato: 192
Eliminato: 187
Eliminato: 8
Eliminato: 3
Eliminato: 22
Eliminato: 187
Eliminato: 199
Eliminato: slightly smaller
Eliminato: 187
Eliminato: 194
Eliminato: higher extremes estimates than parametric methods

return levels < 30 y (for GEV and GPD) and < 50 y (PP) already in 2050 for Venice. For Marseille, events that currently have a return level above 200 y are projected to have return levels < 30 y (for GEV and GPD) and < 100 y (PP) already in 2050.

Eliminato: .

4. Discussion

4.1 Including non-stationarity in extreme events modeling

Our results show that most of the fitted ESL models benefit from the inclusion of covariates on either the location and the scale parameters. We used only the yearly averaged mean sea level as covariate to build simple models, but other predictors can be used. For instance, the North Atlantic Oscillation Index, the Arctic Oscillation, the East Atlantic/Western Russia Oscillation index can be used to include a dependence from climate (Menéndez and Woodworth, 2010). Where climatic predictors are missing, seasonality effects can be included e.g. with an harmonic dependences from the yearly Julian day (Méndez et al., 2006). Other predictors could include global and regional meteorological parameters, which could influence storm surges intensities and frequencies (Grinsted et al., 2013). A dependence from time can be also included (Mudersbach and Jensen, 2010). However, particular care should be used in the choice of the predictors. Complex models can be useful for explaining historical pattern, but might be of little utility for future projections. For instance, bias could arise due to uncertainties in predictor's future trajectories, or to future predictor's values out of the ranges used to calibrate the models. In this regard, simpler models can be helpful for future projections when clear links between extremes occurrence and specific predictor's classes are established.

In this work, we used the mean sea level as covariate because of the strong link with storm surges occurrences (Lionello et al., 2021). Our results show that mean sea level-dependent location of both GEV and PP models improve the ESLs fit. The location parameter is the first-order moment of the extremes distributions. The inclusion of a linear dependence from the mean sea level translates rigidly the distribution function towards higher (positive slope) or lower (negative slope) values without affecting the shape of the distribution. GEV and PP models also marginally improved with a dependence on the scale. The scale parameter relates to the second-order moment of the distribution (the "spreading"): the dependence could suggest that the mean sea level influences also the variability in the storm surge magnitude. In shallow area an higher sea level corresponds to lower dissipation of the tidal energy, yielding higher ESLs (Arns et al., 2017). In the Venice lagoon, this factor might be influenced also by the morphological transformations that the Venice Lagoon underwent during the 20th century and that might have affected the dynamics of the tide propagation (Caruso and Marani, 2022). Different explanations for this pattern are possible. For instance, the North Atlantic Oscillation Index (NAO), not included in this analysis, might act as a latent variable: negative NAO phases in the Mediterranean basin can lead to increases in monthly mean sea levels and in the number of storms (Cid et al., 2016).

Eliminato: mean

Overall, this work shows how including non-stationarity in extreme events analysis can support an improved understanding of extreme events. Including dependences from the mean sea levels allows for flexible forecasts of ESLs also under sea level rise scenarios.

4.2 Comparison of the models

The significant covariate dependencies could be also influenced by the used type of data. The BM data show clear increasing trends, which were captured by the GEV model. BM could be extracted with different methods, such as monthly blocks, or for r-largest yearly values. A global analysis (Wahl et al., 2017) showed that the annual maxima is the more conservative method (i.e. yields higher return period estimates). However, this aspect should be checked as part of a sensitivity analysis from case to case. POT data do not have a trend in the mean or in the higher quantiles, thus should yield models that are less affected by non-stationarity. However, a trend in the frequency of occurrences of POT (Ferrarin et al., 2022) was observed, which might invalidate the homogeneity assumptions of GDP and PP models. The non-homogeneity of the POT distribution can be mitigated by introducing a dependence of the threshold from a covariate (Roth et al., 2012). However, using a non-constant threshold introduces a significant uncertainty that might result in biased estimates of the return levels (Agilan et al., 2021). On the contrary, the PP explicitly models the rate of threshold exceedances: the detected significant dependence of location from the mean sea level implies a process with non-constant occurrence rate (i.e. a non-homogeneous process, eq. 6, Cid et al., 2016).

While all the parametric methods improved with the inclusion of non-stationarity, the JPM is the method that should be least influenced by non-stationarity, since the methodology requires to detrend the data before the calculation of tide and surge histograms. However, as the residual trend on detrended BM for Venice shows, the removal of the mean sea level might not be sufficient to make the series stationary. Thus, also estimates of the return level with the JPM might be biased. Estimations of return levels for long return periods are not possible due to the lack of surge and tide events that are needed to populate the extremal classes of the distribution. In our analysis, JPM allows for estimating return periods corresponding to levels of + 233 cm in Venice (corresponding to the sum of the maximum recorded tide, + 57 cm, the maximum recorded surge, + 141 cm, and the current mean sea level, + 35 cm) and + 163 cm in Marseille (tide: + 20 cm, surge: + 89 cm, current mean sea level: + 54 cm), but for shortest series, this limitation might be stronger.

All the parametric models were improved by the inclusion of covariates on the location (GEV and PP) or on the scale (GPD), with a stronger influence on models fitted to non detrended data. Particular care should be taken when detrending data prior to the model fit, as this action implicitly assumes that the mean sea level is the main responsible of data non-stationarity, and higher order interactions are neglected. In shallow area this could not be the case (Arns et al., 2017). Thus, inclusion of covariates on the model's parameters could be an alternative to detrending in such cases. With our data, the use of the mean sea level as covariate results in a rigid translation towards higher return levels for GEV and PP plots due to the significance of the location dependence. The effect on GPD is also in a change in slope due to the significance of the scale parameter.

Formattato: Non Evidenziato

Eliminato: of up to 150 years without extrapolation

Eliminato: . Among all the analyzed methods, the JPM yields the most conservative estimates of return levels. This is due to the fact that combinations of tide and surge that did not occurred but are virtually possible, are used in the convolution (Pugh and Vassie, 1978).

Data from different gauging stations might show different behaviors. For instance, sites where the sea level variability increases with mean sea level might show a significant dependence in the scale parameter also in GEV and PP.

Overall, we show that using different methods allows to critically examine strengths and weaknesses of each method and to critically evaluate the results to drive the choice of the method that best fits the specific case.

Conclusions

In this paper, we fitted different extreme value models to long-term sea level data. We show that including non-stationarity in the analysis of extreme events improves the fit of most of the models. Non-stationary analyses also yield higher estimates of long-term return levels, while stationary analysis on non-detrended data underestimates the return levels. Overall, we show that non-stationary extremes analyses can provide more robust estimates of return levels to be used in coastal protection planning.

Eliminato: .

Aknowledgements

This work was supported by the EU-INTERREG project ADRIACLIM (grant number IT-HR 10252001)

Data availability

Sea level data from Venice used in this work are freely available in the web portal of the Italian Institute for Environmental Protection and Reaserch (ISPRA): https://www.venezia.isprambiente.it/rete-meteo-mareografica. Sea level data from Marseille were accessed through the IOC portal at: http://www.ioc-sealevelmonitoring.org/ssc/stationdetails.php?id=SSC-mars.

Eliminato: Data

Eliminato: https://www.venezia.isprambiente.it/rete-meteo-mareografica

Author contributions

SM and DB designed the study and implemented the models. FC and EC collected the data. DB led the writing of the manuscript with inputs from all co-authors.

Competing interests

The authors declare that they have no conflict of interest.

References

Agilan, V., Umamahesh, N. V., and Mujumdar, P. P.: Influence of threshold selection in modeling peaks over threshold based nonstationary extreme rainfall series, J. Hydrol., 593, 125625, https://doi.org/10.1016/j.jhydrol.2020.125625, 2021.

Arns, A., Wahl, T., Dangendorf, S., and Jensen, J.: The impact of sea level rise on storm surge water levels in the northern part of the German Bight, Coast. Eng., 96, 118–131, https://doi.org/10.1016/j.coastaleng.2014.12.002, 2015.

Arns, A., Dangendorf, S., Jensen, J., Talke, S., Bender, J., and Pattiaratchi, C.: Sea-level rise induced amplification of coastal protection design heights, Sci. Rep., 7, 1–9, https://doi.org/10.1038/srep40171, 2017.

Bernier, N. B., Thompson, K. R., Ou, J., and Ritchie, H.: Mapping the return periods of extreme sea levels : Allowing for short sea level records , seasonality , and climate change, 57, 139–150, https://doi.org/10.1016/j.gloplacha.2006.11.027, 2007.

Biasio, F. De, Baldin, G., and Vignudelli, S.: Revisiting Vertical Land Motion and Sea Level Trends in the Northeastern Adriatic Sea Using Satellite Altimetry and Tide Gauge Data, 1–25, 2020.

Boettle, M., Rybski, D., and Kropp, J. P.: Quantifying the effect of sea level rise and flood defence – A point process perspective on coastal flood damage, Nat. Hazards Earth Syst. Sci., 16, 559–576, https://doi.org/10.5194/nhess-16-559-2016, 2016.

Carniello, L., Defina, A., and D'Alpaos, L.: Morphological evolution of the Venice lagoon: Evidence from the past and trend for the future, J. Geophys. Res. Earth Surf., 114, 1–10, https://doi.org/10.1029/2008JF001157, 2009.

Caruso, M. F. and Marani, M.: Extreme-coastal-water-level estimation and projection : a comparison of statistical methods, 1109–1128, 2022.

Castillo, E., Hadi, A. S., Balakrishnan, N., and Sarabia, J.-M.: Extreme value and related models with applications in engineering and science, 2005.

Cebrián, A. C., Abaurrea, J., and Asín, J.: NHPoisson: An R package for fitting and validating nonhomogeneous Poisson processes, J. Stat. Softw., 64, 1–25, 2015.

Cid, A., Menéndez, M., Castanedo, S., Abascal, A. J., Méndez, F. J., and Medina, R.: Long-term changes in the frequency, intensity and duration of extreme storm surge events in southern Europe, Clim. Dyn., 46, 1503–1516, https://doi.org/10.1007/s00382-015-2659-1, 2016.

Coles, S., Bawa, J., Trenner, L., and Dorazio, P.: An introduction to statistical modeling of extreme values, Springer, 2001.

Devlin, A. T., Pan, J., and Lin, H.: Extended Water Level Trends at Long-Record Tide Gauges Via Moving Window Averaging and Implications for Future Coastal Flooding, J. Geophys. Res. Ocean., 126, e2021JC017730, 2021.

Dixon, M. J. and Tawn, J. A.: The effect of non-stationarity on extreme sea-level estimation, J. R. Stat. Soc. Ser. C Appl. Stat., 48, 135–151, https://doi.org/10.1111/1467-9876.00145, 1999.

Ferrarin, C., Lionello, P., Orlić, M., Raicich, F., and Salvadori, G.: Venice as a paradigm of coastal flooding under multiple compound drivers, Sci. Rep., 1–11, https://doi.org/10.1038/s41598-022-09652-5, 2022.

Garner, G. G., Hermans, T., Kopp, R. E., Slangen, A. B. A., Edwards, T. L., Levermann, A., and Pearson, B.: Framework for assessing changes to sea-level (facts), IPCC ar6 sea-level rise projections, version 20210809, 2021.

Gilleland, E. and Katz, R. W.: extRemes 2.0: An Extreme Value Analysis Package in R, J. Stat. Softw., 72, 1–39, https://doi.org/10.18637/JSS.V072.I08, 2016.

Grinsted, A., Moore, J. C., and Jevrejeva, S.: Projected Atlantic hurricane surge threat from rising temperatures, 110, https://doi.org/10.1073/pnas.1209980110, 2013.

Jongman, B., Ward, P. J., and Aerts, J. C. J. H.: Global exposure to river and coastal flooding: Long term trends and changes, Glob. Environ. Chang., 22, 823–835, https://doi.org/10.1016/j.gloenvcha.2012.07.004, 2012.

Kelley, D. E.: Oceanographic analysis with R, Springer, 2018.

Khaliq, M. N., Ouarda, T. B. M. J., Ondo, J. C., Gachon, P., and Bobée, B.: Frequency analysis of a sequence of dependent and/or non-stationary hydro-meteorological observations: A review, J. Hydrol., 329, 534–552, https://doi.org/10.1016/J.JHYDROL.2006.03.004, 2006.

Kron, W.: Coasts: The high-risk areas of the world, Nat. Hazards, 66, 1363–1382, https://doi.org/10.1007/s11069-012-0215-4, 2013.

Lionello, P., Barriopedro, D., Ferrarin, C., Nicholls, R. J., Orlić, M., Raicich, F., Reale, M., Umgiesser, G., Vousdoukas, M., and Zanchettin, D.: Extreme floods of Venice: Characteristics, dynamics, past and future evolution (review article), Nat. Hazards Earth Syst. Sci., 21, 2705–2731, https://doi.org/10.5194/nhess-21-2705-2021, 2021.

Marcos, M., Tsimplis, M. N., and Shaw, A. G. P.: Sea level extremes in southern Europe, 114, 1–16, https://doi.org/10.1029/2008JC004912, 2009.

Masina, M. and Ciavola, P.: Analisi dei livelli marini estremi e delle acque alte lungo il litorale ravennate, Stud. costieri, 18, 87–101, 2011.

Masson-Delmotte, V., Zhai, P., Pirani, A., Connors, S. L., Péan, C., Berger, S., Caud, N., Chen, Y., Goldfarb, L., and Gomis, M. I.: Climate Change 2021: The Physical Science Basis. Contribution of Working Group I to the Sixth Assessment Report of the Intergovernmental Panel on Climate Change, IPCC Geneva, Switz., 2021.

Méndez, F. J., Menéndez, M., Luceño, A., and Losada, I. J.: Estimation of the long-term variability of extreme significant wave height using a time-dependent Peak Over Threshold (POT) model, J. Geophys. Res. Ocean., 111, https://doi.org/10.1029/2005JC003344, 2006.

Méndez, F. J., Menéndez, M., Luceño, A., and Losada, I. J.: Analyzing monthly extreme sea levels with a time-dependent GEV model, J. Atmos. Ocean. Technol., 24, 894–911, 2007.

Menéndez, M. and Woodworth, P. L.: Changes in extreme high water levels based on a quasi-global tide-gauge data set, J. Geophys. Res. Ocean., 115, 1–15, https://doi.org/10.1029/2009JC005997, 2010.

Mentaschi, L., Vousdoukas, M., Voukouvalas, E., Sartini, L., and Feyen, L.: The transformed-stationary approach : a generic and simplified methodology for non-stationary extreme value analysis, 3527–3547, https://doi.org/10.5194/hess-20-3527-2016, 2016.

Mudersbach, C. and Jensen, J.: Nonstationary extreme value analysis of annual maximum water levels for designing coastal structures on the German North Sea coastline, J. Flood Risk Manag., 3, 52–62, https://doi.org/10.1111/j.1753-318X.2009.01054.x, 2010.

Pugh, D. T. and Vassie, J. M.: Extreme sea levels from tide and surge probability, in: Coastal Engineering, 911–930, 1978.

R Core Team: R: A Language and Environment for Statistical Computing, https://www.r-project.org/, 2021.

Raicich, F., Orlic, M., and Malacic, V.: A case study of the Adriatic seiches (December 1997), Nuovo Cim. della Soc. Ital. di Fis. C, 22, 1999.

Razmi, A., Golian, S., and Zahmatkesh, Z.: Non-Stationary Frequency Analysis of Extreme Water Level : Application of Annual Maximum Series and Peak-over Threshold Approaches, 2065–2083, https://doi.org/10.1007/s11269-017-1619-4, 2017.

Roth, M., Buishand, T. A., Jongbloed, G., Klein Tank, A. M. G., and Van Zanten, J. H.: A regional peaks-over-threshold model in a nonstationary climate, Water Resour. Res., 48, 1–12, https://doi.org/10.1029/2012WR012214, 2012.

Salas, J. D. and Obeysekera, J.: Revisiting the concepts of return period and risk for nonstationary hydrologic extreme events, J. Hydrol. Eng., 19, 554–568, 2014.

Sweet, W. V and Park, J.: From the extreme to the mean: Acceleration and tipping points of coastal inundation from sea level rise, Earth's Futur., 2, 579–600, 2014.

Tebaldi, C., Strauss, B. H., and Zervas, C. E.: Modelling sea level rise impacts on storm surges along US coasts, https://doi.org/10.1088/1748-9326/7/1/014032, 2012.

Tebaldi, C., Ranasinghe, R., Vousdoukas, M., Rasmussen, D. J., Vega-Westhoff, B., Kirezci, E., Kopp, R. E., Sriver, R., and Mentaschi, L.: Extreme sea levels at different global warming levels, Nat. Clim. Chang., 11, 746–751, 2021.

Umgiesser, G., Bajo, M., Ferrarin, C., Cucco, A., Lionello, P., Zanchettin, D., Papa, A., Tosoni, A., Ferla, M., Coraci, E., Morucci, S., Crosato, F., Bonometto, A., Valentini, A., Orlić, M., Haigh, I. D., Nielsen, J. W., Bertin, X., Fortunato, A. B., Pérez Gómez, B., Alvarez Fanjul, E., Paradis, D., Jourdan, D., Pasquet, A., Mourre, B., Tintoré, J., and Nicholls, R. J.: The prediction of floods in Venice: Methods, models and uncertainty (review article), Nat. Hazards Earth Syst. Sci., 21, 2679–2704, https://doi.org/10.5194/nhess-21-2679-2021, 2021.

Valle-Levinson, A., Marani, M., Carniello, L., D'Alpaos, A., and Lanzoni, S.: Astronomic link to anomalously high mean sea level in the northern Adriatic Sea, Estuar. Coast. Shelf Sci., 257, 107418, https://doi.org/10.1016/j.ecss.2021.107418, 2021.

Vousdoukas, M. I., Voukouvalas, E., Annunziato, A., Giardino, A., and Feyen, L.: Projections of extreme storm surge levels along Europe, Clim. Dyn., 47, 3171–3190, https://doi.org/10.1007/s00382-016-3019-5, 2016.

Wahl, T., Haigh, I. D., Nicholls, R. J., Arns, A., Dangendorf, S., Hinkel, J., and Slangen, A. B. A.: Understanding extreme sea levels for broad-scale coastal impact and adaptation analysis, Nat. Commun., 8, 1–12, https://doi.org/10.1038/ncomms16075, 2017.

Zanchettin, D., Bruni, S., Raicich, F., Lionello, P., Adloff, F., and Androsov, A.: Sea-level rise in Venice : historic and future trends (review article), 2643–2678, 2021.

Zhang, K., Douglas, B. C., and Leatherman, S. P.: Twentieth-century storm activity along the US east coast, J. Clim., 13, 1748–1761, 2000.

Cheng, L., Aghakouchak, A., Gilleland, E., Katz, R.W., 2014. Non-stationary extreme value analysis in a changing climate 353–369. https://doi.org/10.1007/s10584-014-1254-5

Haigh, I.D., Nicholls, R., Wells, N., 2010. A comparison of the main methods for estimating probabilities of extreme still water levels. Coast. Eng. 57, 838–849. https://doi.org/10.1016/j.coastaleng.2010.04.002

Letetrel, C., Marcos, M., Martín Míguez, B., Woppelmann, G., 2010. Sea level extremes in Marseille (NW Mediterranean) during 1885-2008. Cont. Shelf Res. 30, 1267–1274. https://doi.org/10.1016/j.csr.2010.04.003

Ragno, E., Aghakouchak, A., Cheng, L., Sadegh, M., 2019. Advances in Water Resources A generalized framework for process-informed nonstationary extreme value analysis. Adv. Water Resour. 130, 270–282. https://doi.org/10.1016/j.advwatres.2019.06.007

Tawn, J.A., Vassie, J.M., Gumbel, E.J., 1989. Extreme sea levels; the joint probabilities method revised and refined. Proc. Inst. Civ. Eng. 87, 429–442. https://doi.org/https://doi.org/10.1680/iicep.1989.2975

Wöppelmann, G., Marcos, M., Coulomb, A., Martín Míguez, B., Bonnetain, P., Boucher, C., Gravelle, M., Simon, B., Tiphaneau, P., 2014. Rescue of the historical sea level record of Marseille (France) from 1885 to 1988 and its extension back to 1849-1851. J. Geod. 88, 869–885. https://doi.org/10.1007/s00190-014-0728-6

Zanchettin, D., Bruni, S., Raicich, F., Lionello, P., Adloff, F., Androsov, A., 2021. Sea-level rise in Venice : historic and future trends (review article) 2643–2678.

Formattato: Rientro: Sinistro: 0 cm, Prima riga: 0 cm, Controlla righe isolate, Regola lo spazio tra testo asiatico e in alfabeto latino, Regola lo spazio tra caratteri asiatici e numeri

Formattato: Giustificato, Interlinea: 1,5 righe

Eliminato: ¶

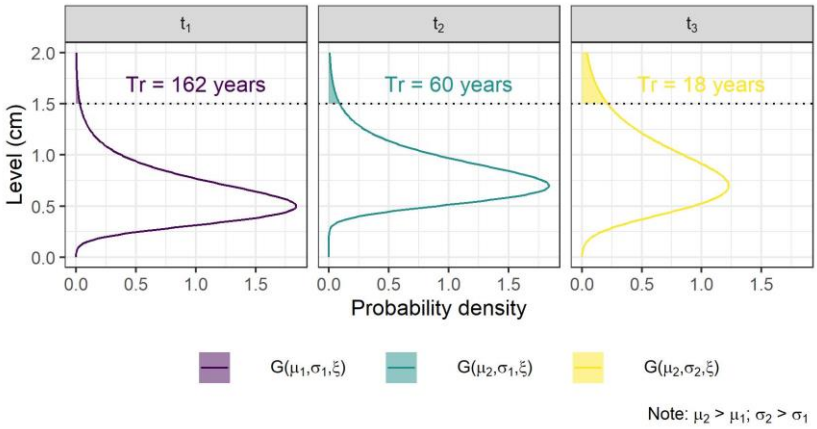

570

Figure 1: Example of the effects of curves parameters on the return period estimation. GEV curves with different location (μ) and scale (σ) parameters corresponding to three time periods are represented. The shape (ξ) parameter is kept constant The return period is calculated based on the highlighted area (see section 2.3.7). Different location and scale yield different return period estimates. Under non-stationary conditions, the curve's parameters change with time.

575

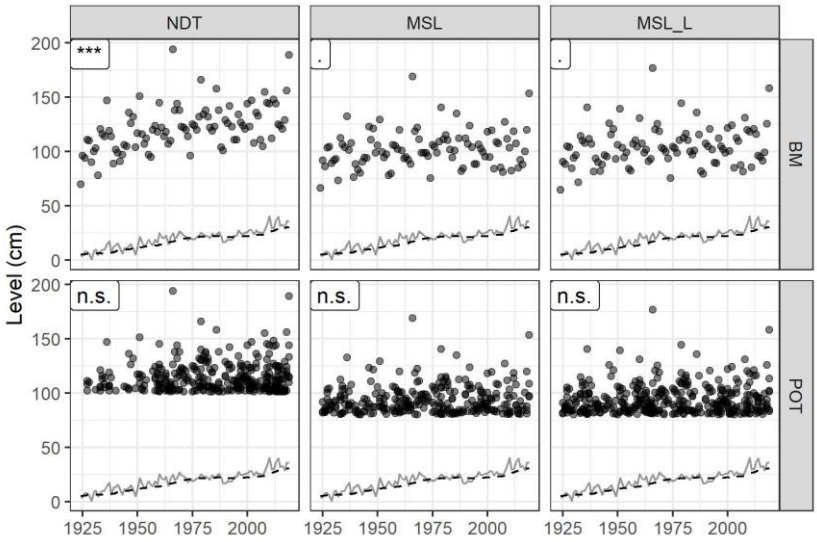

Figure 2: Venice tide gauge data used to fit the models. Plots are grouped vertically according to the detrending method (MSL: mean sea level, MSL_L: long term mean sea level, NDT: non detrended), and horizontally according to the maxima typology (BM: block maxima, POT: peak over threshold). The text in the label on the top-left corner of each plot shows the significance level of the Mann-Kendall trend test (n.s.: non significant; .: p < 0.1; *: p < 0.05; **: p < 0.01; ***: p < 0.001). The continuous line represents the mean sea level value; the dashed line represents the long-term mean sea level.

Eliminato: D

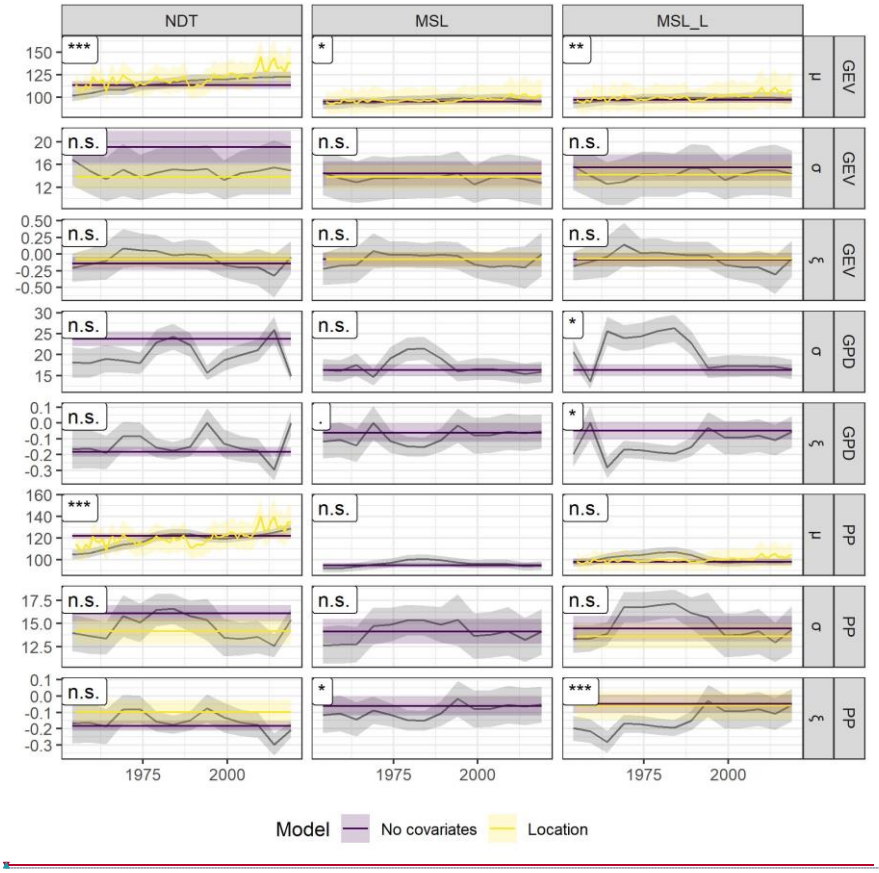

Figure 3: Comparison between the parameters estimated in the time window analysis (full thin line; the grey envelope represents the uncertainty of the parameters from the time window analysis) and the parameters estimated by different models configurations over the full data length. Parameters from all the configurations of GEV, GPD and PP that do not include covariates are showed. Parameters from models with covariates are showed only if models improve significantly the fit (see Table 2 for the likelihood test). The shape ξ is included in the figure, but no covariates dependence was tested for this parameter. The horizontal axis represents the final year of the time window. Plots are grouped vertically according to the detrending method (MSL: mean sea level, MSL_L: long term mean sea level, NDT: non detrended), and horizontally according to the distribution function (GEV: generalized extreme values, GPD: generalized pareto, PP: point process). The text in the label on the top-left corner of each plot shows the significance level of the Mann-Kendall trend test on the parameters from the time-window analysis (n.s.: non significant; .: p < 0.1; *: p < 0.05; **: p < 0.01; ***: p < 0.001).

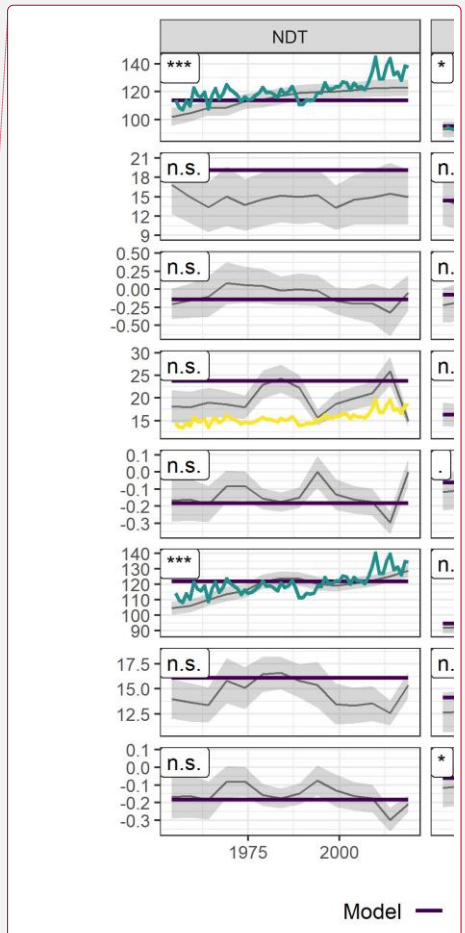

Eliminato:

Formattato: Tipo di carattere: 12 pt

Eliminato: with gray

Eliminato: the

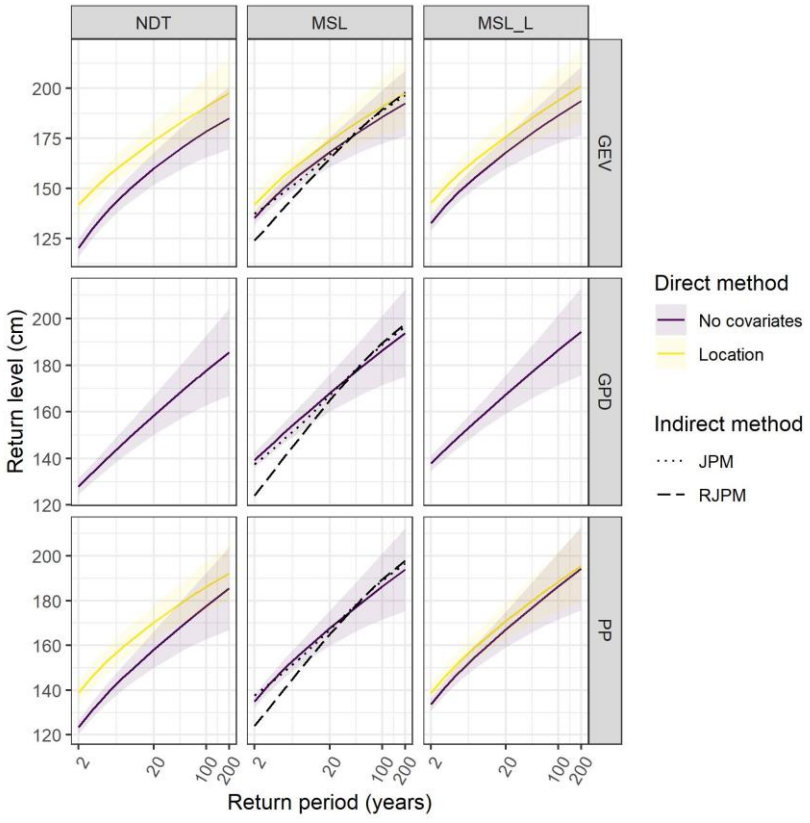

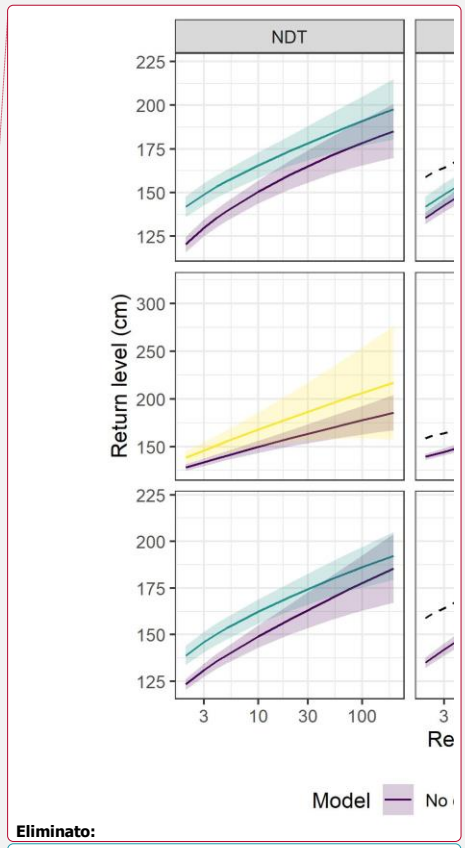

Eliminato:

Formattato: Tipo di carattere: 12 pt

Figure 4: Return level plot actualized to 2019 for Venice. Plots are grouped vertically according to the detrending method (MSL: mean sea level, MSL_L: long term mean sea level, NDT: non detrended), and horizontally according to the distribution function (GEV: generalized extreme values, GPD: generalized pareto, PP: point process). The dashed line is the empirical return level for the joint probability method (JPM). Curves are color-coded based on the model configuration. Note: horizontal axis is logarithmic. Return level curves for direct models with covariates are showed only if the addition of the covariate improves the fit significantly ($p < 0.01$; see Table 2).

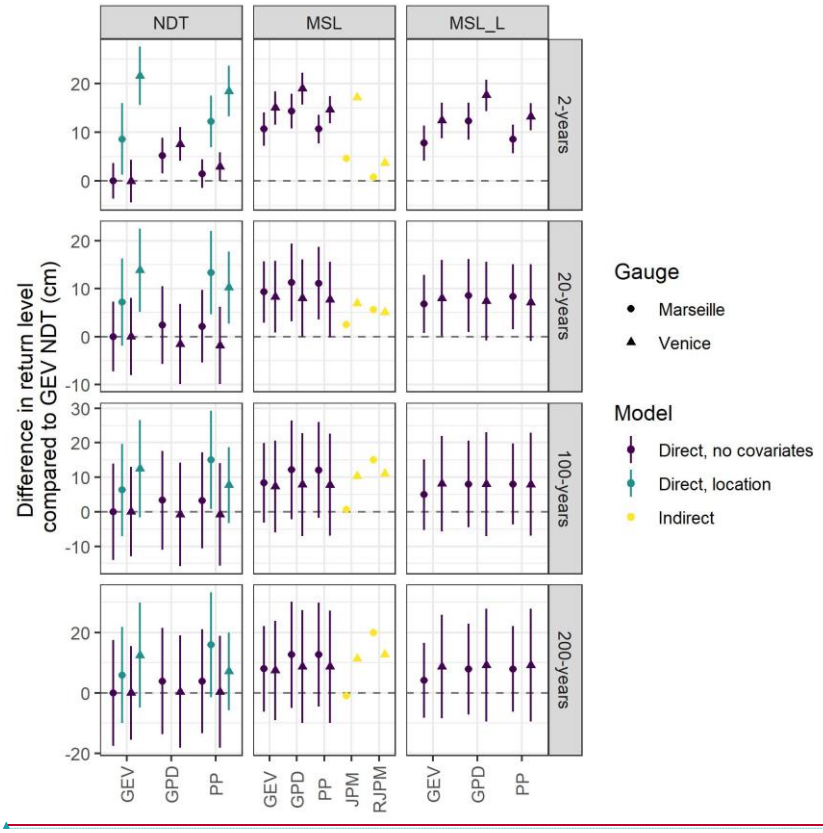

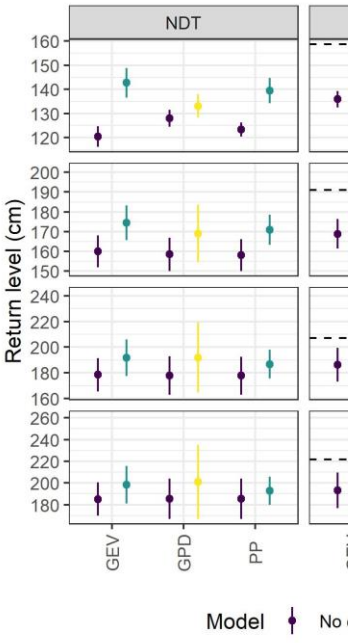

Figure 5: Difference of return levels between each fitted model and a non-detrended, GEV fit for different return periods. Return levels of models with covariates are showed only if the model significantly improves the fit compared to models without covariates ($p < 0.01$; see Table 2). Plots are grouped vertically according to the detrending method (MSL: mean sea level, MSL_L: long term mean sea level, NDT: non detrended), and horizontally according to the distribution function (GEV: generalized extreme values, GP: generalized pareto, PP: point process).

Eliminato:

Formattato: Tipo di carattere: 12 pt

Eliminato: Estimates

Eliminato:

Eliminato: The horizontal dashed line is the return level for the joint probability method. Estimates from the GPD with covariates on the scale are not reported because those models are not significantly improving the stationary version. Return levels from models fitted to non-detrended data without covariates are reported for completeness since they do not account for non stationarity.

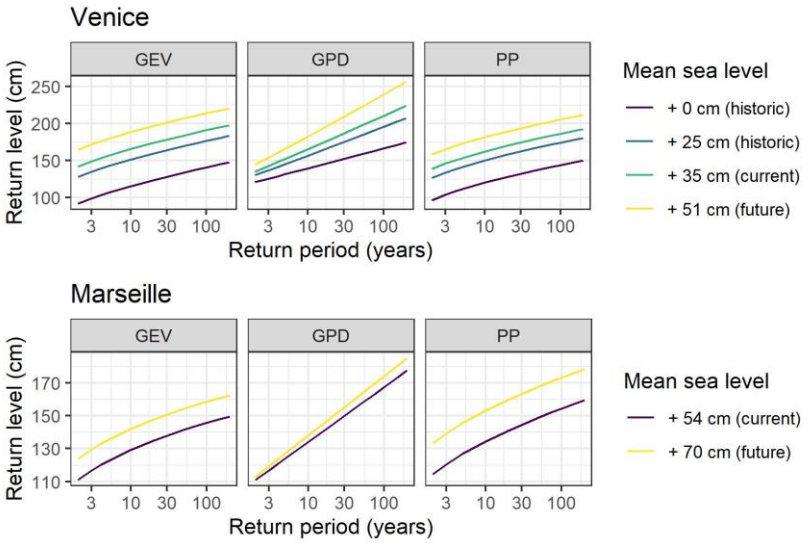

Figure 6: Return level plots for different values of mean sea level. Mean sea level is expressed with respect to the local reference. Current mean sea level is + 35 for Venice and + 54 for Marseille. See section 2.4 for a description of the selected future mean sea levels.

Table 1: Trend in the data used to fit the models. lm: linear model; qr: quantile regression (0.75th data quantile).

Detrending	Extreme selection method	Regression Type	Regression type	Test statistic	R^2
NDT	BM	lm	F(1,94) = 61.089	p = 7.75 10^{-12}***	0.38
NDT	POT	lm	F(1,317) = 3.265	p = 0.071.	0.007
NDT	POT	qr	F(1,317) = 2.733	p = 0.099.	-
MSL	BM	lm	F(1,94) = 7.662	p = 0.006**	0.06
MSL	POT	lm	F(1,282) = 2.417	p = 0.12n.s.	0.004
MSL	POT	qr	F(1,282) = 1.102	p = 0.29n.s.	-
MSL_L	BM	lm	F(1,94) = 14.276	p = 2.76 10^{-5}***	0.12
MSL_L	POT	lm	F(1,357) = 5.432	p = 0.020*	0.01
MSL_L	POT	qr	F(1,357) = 5.058	p = 0.025*	-

Table 2: Likelihood ratio test results. The column test type describes which models configurations were compared: nc-l no covariates compared with covariates on location, l-sl: covariates on the location compared with covariates on both location and scale, nc-s no covariates compared with covariates on scale. VE = Venice; MS = Marseille.

Detrending	Distribution	Test Type	Test Statistic VE	p-value VE	Test Statistic MS	p-value MS
NDT	GEV	nc-l	chisq2(1) = 53.582	2.48 10^{-13}***	chisq2(1) = 6.395	0.011*
NDT	GEV	l-sl	chisq2(1) = 1.141	0.28n.s.	chisq2(1) = 0.109	0.74n.s.
NDT	GPD	nc-s	chisq2(1) = 3.958	0.046*	chisq2(1) = 0.175	0.67n.s.
NDT	PP	nc-l	chisq2(1) = 122.945	1.43 10^{-28}***	chisq2(1) = 43.768	3.69 10^{-11}***
NDT	PP	l-sl	chisq2(1) = 3.799	0.051.	chisq2(1) = 0.346	0.55n.s.
MSL	GEV	nc-l	chisq2(1) = 6.903	0.008**	chisq2(1) = 0.379	0.53n.s.
MSL	GEV	l-sl	chisq2(1) = 1.141	0.28n.s.	chisq2(1) = 0.11	0.73n.s.
MSL	GPD	nc-s	chisq2(1) = 3.358	0.06.	chisq2(1) = 0.003	0.95n.s.
MSL	PP	nc-l	chisq2(1) = 3.078	0.079.	chisq2(1) = 0.123	0.72n.s.
MSL	PP	l-sl	chisq2(1) = 3.086	0.078.	chisq2(1) = 0.001	0.97n.s.
MSL_L	GEV	nc-l	chisq2(1) = 13.887	1.94 10^{-4}***	chisq2(1) = 0.099	0.75n.s.
MSL_L	GEV	l-sl	chisq2(1) = 1.063	0.30n.s.	chisq2(1) = 0.084s.	0.77n.s.
MSL_L	GPD	nc-s	chisq2(1) = 6.213	0.012*	chisq2(1) = 0.005	0.94n.s.
MSL_L	PP	nc-l	chisq2(1) = 13.42	2.48 10^{-4}***	chisq2(1) = 7.087	0.007**
MSL_L	PP	l-sl	chisq2(1) = 4.878	0.027*	chisq2(1) = 0.601.	0.43n.s.

Formattato ...
Formattato ...
Formattato ...
Eliminato: p =
Formattato ...
Formattato ...
Formattato ...
Formattato ...
Formattato ...
Formattato ...
Formattato ...
Formattato ...
Eliminato: p =
Formattato ...
Formattato ...
Formattato ...
Formattato ...
Eliminato: p =
Formattato ...
Formattato ...
Formattato ...
Formattato ...
Formattato ...
Formattato ...
Eliminato: p =
Formattato ...
Eliminato: 3
Formattato ...
Formattato ...
Formattato ...
Formattato ...
Formattato ...
Eliminato: p =
Formattato ...
Formattato ...
Formattato ...
Formattato ...
Formattato ...
Formattato ...
Eliminato: p =
Formattato ...
Formattato ...
Formattato ...
Formattato ...
Formattato ...

Table 3: Comparisons between the rates fitted by the point process (PP) for Venice and the empirical process rate of models with covariates on the location (Model Type = l), and models with covariates on location and scale (Model Type = s)

Detrending	Model Type	Test statistic	p-value	R2
NDT	l	t(94) = 12.092	$p = 7.37\ 10^{-21}$***	0.78
NDT	ls	t(94) = 12.344	$p = 2.22\ 10^{-21}$***	0.78
MSL	l	t(94) = 1.8	p = 0.07.	0.18
MSL	ls	t(94) = 1.754	p = 0.08.	0.17
MSL_L	l	t(94) = 3.608	$p = 4.97\ 10^{-4}$***	0.34
MSL_L	ls	t(94) = 3.451	$p = 8.39\ 10^{-4}$***	0.33